ACS OMEGA

http://pubs.acs.org/journal/acsodf

Article

Retention Improvement of HZO-Based Ferroelectric Capacitors with TiO_2 Insets

Aleksandra A. Koroleva, Anna G. Chernikova, Sergei S. Zarubin, Evgeny Korostylev, Roman R. Khakimov, Maksim Yu. Zhuk, and Andrey M. Markeev*

Cite This: *ACS Omega* 2022, 7, 47084−47095

Read Online

ACCESS | Metrics & More | Article Recommendations | Supporting Information

ABSTRACT: The influence of the bottom TiO_2 interfacial layer grown by atomic layer deposition on the ferroelectric properties of the TiN/$Hf_{0.5}Zr_{0.5}O_2$/TiN capacitors is systematically investigated. We show that the integration of the TiO_2 layer leads to an increase in the polar orthorhombic phase content in the $Hf_{0.5}Zr_{0.5}O_2$ film. In addition, the crystalline structure of the $Hf_{0.5}Zr_{0.5}O_2$ film is highly dependent on the thickness of the TiO_2 inset, with monoclinic phase stabilization after the increase of TiO_2 thickness. Special attention in this work is given to the key reliability parameters—retention and endurance. We demonstrate that the integration of the TiO_2 inset induces valuable retention improvement. Using a novel approach to the depolarization measurements, we show that the depolarization contribution to the retention loss is insignificant, which leaves the imprint effect as the root of the retention loss in TiN/TiO_2/$Hf_{0.5}Zr_{0.5}O_2$/TiN devices. We believe that the integration of the insulator interfacial layer suppresses the scavenging effect from the bottom TiN electrode, leading to a decrease in the oxygen vacancy content in the $Hf_{0.5}Zr_{0.5}O_2$ film, which is the main reason for imprint mitigation. At the same time, although the observed retention improvement is very promising for the upcoming technological integration, the field cycling testing revealed the endurance limitations linked to the phase transitions in the TiO_2 layer and the rise of the effective electric field applied to the $Hf_{0.5}Zr_{0.5}O_2$ film.

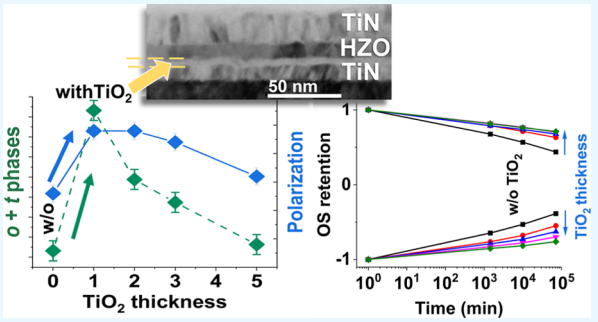

1. INTRODUCTION

Ferroelectricity in doped HfO_2 films[1] was thoroughly researched in the last decade due to their ultimate scalability[2] and CMOS compatibility.[3] Although ferroelectricity can be achieved in HfO_2 by the incorporation of various dopants, including Si,[4] Al[5], La,[6] Y,[7] and so forth, the $Hf_{0.5}Zr_{0.5}O_2$ (HZO) mixed oxide drew the highest attention due to the relatively low crystallization temperature (400−600 °C) and, therefore, back-end-of-line (BEOL) compatibility.[8] HZO films are also easily fabricated by atomic layer deposition (ALD), where the necessary Hf/Zr ratio can be achieved by controlling the ratio between the ALD cycles. In addition, utilization of the ALD allows the development of deep-trenched ferroelectric capacitors. In this regard, it is natural to implement ALD for electrode deposition as well. Among ALD-grown electrodes, technologically friendly TiN is the most promising one.[9,10] It was previously demonstrated that the use of the TiN top electrode grown by ALD at T_{dep} = 400 °C allows excluding the postdeposition annealing step usually required for the HZO ferroelectric phase stabilization,[10] which may be useful for the optimization of the device fabrication process. Studies of full ALD TiN/HZO/TiN capacitors show that these structures exhibit a double remanent polarization ($2P_r$) value of 20−25 $\mu C/cm^2$ and a high endurance (more than $4{\cdot}10^{10}$ switching cycles at 2.5 MV/cm).[10,11] However, another key reliability parameter−retention of these structures−has not been properly investigated yet.

Retention, in general, is a complex problem for HfO_2-based capacitors, since a common benchmark of 10 years at 85 °C appears to be difficult to achieve, especially at the BEOL-compatible annealing temperatures.[12] For this reason, finding a way to improve retention without elevation of the annealing temperature is an important task. It is argued that the imprint effect, which is a gradual shift of the hysteresis loop toward a negative or positive electric field depending on the stored polarization direction, is the main reason for the retention loss.[13] However, effects such as relaxation and thermal depolarization can also contribute to retention loss.[14]

Many studies suggest that, similar to the wake-up and fatigue effects,[15] other typical reliability issues of HZO-based capacitors, such as the nature of the imprinting phenomenon

Received: September 27, 2022
Accepted: November 29, 2022
Published: December 7, 2022

https://doi.org/10.1021/acsomega.2c06237
ACS Omega 2022, 7, 47084−47095

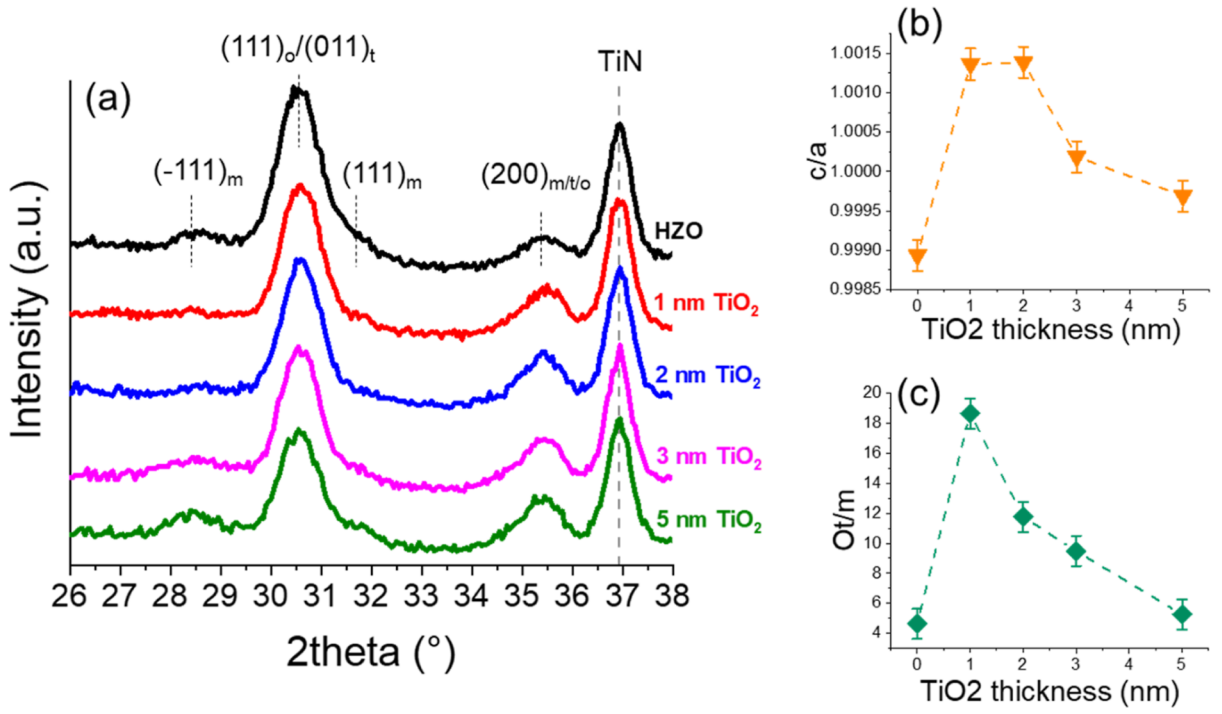

Figure 1. (a) GIXRD collected from TiN/HZO/TiN and TiN/TiO_2/HZO/TiN structures. (b) *c*/*a* value vs the thickness of the TiO_2 inset. (c) Relative ratio of the o/t-phase to m-phase calculated as the integrated area of the peaks as a TiO_2 inset thickness. Lines serve as a guide for the eye.

(and, eventually, retention loss), is related to the oxygen vacancy (V_O) distribution in the HZO film.[16] In addition, a nonferroelectric V_O-rich layer/"dead layer" forms at the TiN/HZO interfaces.[17] According to the interfacial screening model,[18] the existence of a V_O-rich layer leads to the spatial separation between the bound charges in the poled capacitor and the screening charges in the electrodes, leading to the high voltage drop at the dead layer, charge injection through the dead layer to V_O, and, eventually, the imprint effect. Noteworthily, the V_O concentration at the electrode−HZO interface is a hard-to-manage parameter because it can depend on the exact chemical composition of TiN and HZO (e.g., the TiN oxygen content and, eventually, the oxygen-scavenging ability) and interactions between them during growth and postprocessing. It is known that the addition of the interfacial layer at the electrode/insulator interface is a common method used for interface engineering.[19−22] The artificial incorporation of some insulating inset between TiN and HZO, which can be done in a controllable manner, can hinder the aforementioned interactions.

However, interfacial inset dielectric layers are expected to affect the HZO film crystallization process and eventually $2P_r$.[23−29] In this regard, it is worth searching for the insulator inset that leads to improved reliability among such insulators that at least do not diminish the remanent polarization strongly in HZO films. It was demonstrated that integration of the ZrO_2,[26,27] HfO_2,[25] HfO_xN_y,[30,31] or TiO_2[29,32] layer to the bottom interface causes an increase in the relative ratio of the orthorhombic ferroelectric phase, enhancing the ferroelectricity of HZO-based capacitors. Inserting top and bottom TiO_2 layers even allowed achieving ferroelectricity in the as-deposited (T_{dep} = 300 °C) HZO.[33] Gaddam et al. achieved $2P_r$ ≈ 33 μC/cm^2 in the tri-layer TiN/HfO_2/HZO/TiO_2/TiN structures after rapid thermal annealing at a temperature of 350 °C.[34] Lee et al. showed that the integration of the TiO_2 layer at the bottom TiN/HZO interface leads to the point defect-induced stabilization of the ferroelectric HZO phase by promoting the uniform lateral distribution of V_O,[29] which affects the reliability properties of HZO-based capacitors. Kim et al. investigated the endurance of HZO-based capacitors after the ozone treatment of the bottom TiN/HZO interface, achieving ∼10^8 switching cycles at an applied electric field of 3.5 MV/cm without observing a significant wake-up effect or fatigue.[32] However, despite the obvious perspective on using TiO_2, none of the aforementioned studies covers the retention aspect.

In this work, the influence of the bottom interfacial TiO_2 insets on the ferroelectricity of full-ALD TiN/HZO/TiN structures is investigated. We use various TiO_2 thicknesses in the range of ∼1−5 nm since it was previously reported that the thickness of the interfacial TiO_2 layer affects the height and width of the Schottky barrier at the TiN/HZO interface,[12] which in turn may affect the reliability (foremost, imprint, and endurance). We show that the integration of the TiO_2 inset positively affects the retention and imprint in the HZO-based capacitors without serious deterioration of endurance, which makes the TiO_2 insets promising for the potential integration of HZO-based ferroelectric capacitors into the BEOL technology.

2. MATERIALS AND METHODS

Fully grown ALD TiN/TiO_2/HZO/TiN capacitors and TiN/HZO/TiN reference structures with 10 nm thick HZO were investigated in this work. In the case of TiN/TiO_2/HZO/TiN structures, the thicknesses of the bottom TiO_2 insets were ∼1, ∼2, ∼3, and ∼5 nm. In all cases, no additional annealing step was applied because previously it had been proven that the ALD of top TiN (∼20 nm thick) at 400 °C is efficient for the crystallization of the HZO film.[10] The top contacts, with a

https://doi.org/10.1021/acsomega.2c06237
ACS Omega 2022, 7, 47084−47095

diameter of 50 μm, were formed through the lithography process followed by plasma etching.

The crystalline structures of HZO films were investigated by grazing-incidence X-ray diffraction (GIXRD) using an ARL X'TRA equipped with a parabolic mirror and a pinhole collimator with Cu-kα radiation. GIXRD spectra were collected within the 2θ range of 26−38°. To extract the relative content of different phases in HZO, the peaks were fitted with the Gaussian function.

The cross-sections for transmission electron microscopy (TEM) studies were prepared with the focused ion beam technique with the JIB-4501 MultiBeam SEM-FIB System (JEOL, Japan). The thickness and crystalline structure of the layers in this cross-section were investigated with TEM. The bright-field TEM and high-resolution TEM (HRTEM) images were acquired with the JEM-2100 transmission electron microscope (JEOL, Japan) at the 200 kV accelerating voltage. HRTEM and fast Fourier transform diffractograms (FFT) were indexed with the JEMS software.[35]

The positive-up-negative-down (PUND) technique with the triangular voltage sweeps with 10 kHz frequency was used for the switching current versus electric field (I_{sw}−E) curves and remanent polarization versus electric field (P_r−E) hysteresis loop reconstruction before and after the baking of the samples at elevated temperatures. PUND with bipolar trapezoidal cycles and a pulse duration of 3 μs was applied for wake-up and cycling endurance tests. An Agilent B1500A semiconductor parameter analyzer was used for the electric measurements. Voltage was applied to the top electrode, while the bottom electrode was grounded in all kinds of measurements. In the retention measurements, pulses with a duration of 3 μs were used. The pulse scheme and the measurement details are provided in Figure S1 in the Supporting Information.

3. RESULTS AND DISCUSSION

Figure 1a shows the results of GIXRD measurements of the TiN/HZO/TiN and TiN/TiO_2/HZO/TiN structures. All GIXRD spectra contain the TiN (111) reflection at $2\theta \approx 36.9°$ and peaks at $2\theta \approx 30.5°$ and $2\theta \approx 35.4°$, which correspond to $(111)_o/(011)_t$ and $(002)_{o/t}$ reflections of the ferroelectric orthorhombic (space group $Pca2_1$, o-phase) and nonferroelectric tetragonal (space group $P4_2/nmc$, t-phase) phases of HZO, respectively. To analyze the relative amount of the o-phase, the c/a aspect ratio was calculated.[36] Figure 1b shows the relationship between the c/a and TiO_2 film thickness. It can be seen that the introduction of the ∼1 and ∼2 nm thick TiO_2 layers leads to an increase in the c/a value from ∼0.9987 to ∼1.0012. Although the increase is rather small, it indicates a higher o-phase fraction in the HZO films in TiN/TiO_2/HZO/TiN structures with ∼1−2 nm thick TiO_2.[36] Interestingly, a further increase in the TiO_2 layer thickness leads to a decrease in the c/a value, which suggests a relative decrease in the o-phase content and an increase in the t-phase content.

The XRD pattern from the TiN/HZO/TiN structure also shows the $(-111)_m$ and $(111)_m$ reflections related to the formation of the nonferroelectric monoclinic phase (space group $P2_1/_c$, m-phase) at $2\theta \approx 28.4$ and 31.6°, respectively. It can be seen that the introduction of the ∼1 nm thick TiO_2 layer leads to the noticeable suppression of the aforementioned m-phase peaks, while these peaks appear again when the TiO_2 thickness increases. Figure 1c show the relative ratio of the integrated area of the peaks of o/t to m-phase. From this graph, it can also be seen that the m-phase gets suppressed with the addition of the thinnest TiO_2 layer, and then, the m-phase amount gradually increases again.

It is rather challenging to delve into the reasons for such a dependence on the crystalline structure of HZO and the presence of TiO_2 at the bottom interface and its thickness. Qi et al.[33] reported a possible crystallographic orientation relationship between the $(002)_{t\text{-phase}}$ of the HZO film and (110) of TiO_2 in the anatase structure originating from a similar interplanar d-spacing. In addition, the calculations of tensile stress also suggested the local epitaxial growth of a fraction of o-phase HZO grains on TiO_2 anatase grains.[33] The increase in the average tensile stress caused by the integration of TiO_2 was also reported by Gaddam et al.[34] Another reason for the more effective o-phase stabilization can be the adoption of tetragonal-like oxygen coordination during the adsorption of the Hf reactant on the TiO_2 anatase surface.[29] Note that the formed t-phase is expected to transform relatively easily into the o-phase as a result of subsequent annealing. However, to use any of these interpretations to explain, for example, the higher o-phase content in HZO grown on TiO_2 insets, one has to confirm that TiO_2 is crystallized to the anatase phase, which is challenging due to its small thickness. We investigated the crystalline structure of TiO_2 separately to confirm the anticipated anatase phase formation at the chosen ALD conditions.[37] Figure S2 in the Supporting Information shows the GIXRD of TiO_2 film with an increased film thickness of ∼18 nm grown on TiN. The presented diffractogram shows an intense peak at ∼25.35°, which is attributed to the anatase (101) reflection. However, we have not seen any diffraction peaks from TiO_2 for a much thinner TiO_2 inset (Figure 1a). Because the absence of TiO_2 reflections may be related to its low thickness and low grain sizes, which affect the resolution due to the limited sensitivity of the diffraction tool, we performed TEM measurements. Figure 2a shows the cross-sectional TEM image of the TiN/TiO_2 (5 nm)/HZO/TiN

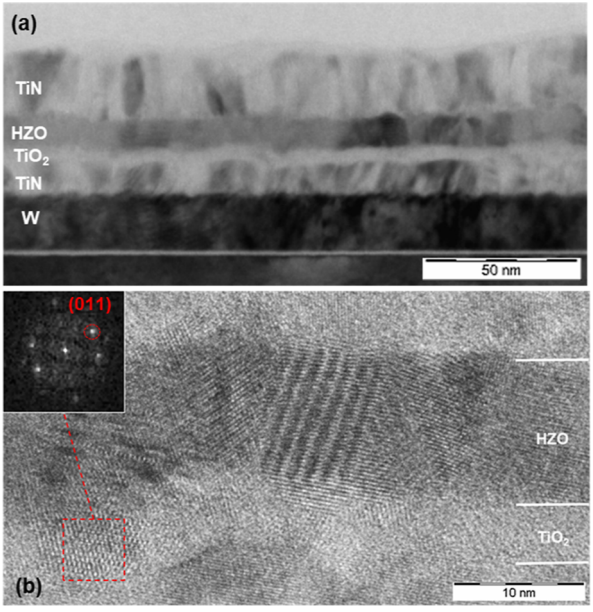

Figure 2. (a) Cross-sectional TEM image of the TiN/TiO_2 (5 nm)/HZO/TiN structure. (b) HRTEM image of the TiO_2/HZO bilayer structure. The inset shows the FFT image from the selected area in the TiO_2 film.

https://doi.org/10.1021/acsomega.2c06237
ACS Omega 2022, 7, 47084−47095

structure. To investigate the crystalline structure of the TiO_2 film, we carried out the HRTEM (Figure 2b) with FFT indexing (inset in Figure 2b), which confirmed the assumed anatase formation at the TiO_2 thickness of ∼5 nm. Previous reports showed that it is possible to grow as thin as ∼1.5 nm TiO_2 by $TiCl_4/H_2O$ ALD on a WO_3 substrate.[38] However, we did not find any signs of crystallization of ∼1−2 nm thick TiO_2 grown on TiN by applying HRTEM to such samples (Figures S3 and S4 in Supporting Information). Thus, the above-presented crystallographic arguments are applicable only to the HZO, grown on relatively thick TiO_2 (3−5 nm) and may explain why the o-phase fraction becomes higher in these samples as compared to the samples with HZO grown directly on TiN. However, it explains neither the observed maximum of the relative o/t to m-phase and o- to t-phase ratios in HZO grown on ultrathin TiO_2 (1−2 nm) nor another increase in the m-phase fraction in HZO grown on thicker TiO_2 (3−5 nm).

Another factor that may affect the crystallization of HZO is the size of the crystalline grains since surface energy contribution is a key factor defining the mutual stability of different crystalline phases in HZO.[39] Previously, Kim et al. showed that integrating the inset layer at the TiN/HZO interface leads to the reduction of the size of HZO grains and explained this phenomenon by the "delayed" nucleation of HZO grains on the amorphous inset layer.[30] Similarly,[30] we obtained the SEM images of the HZO (details are given in Supporting Information, Figure S5) to construct the HZO grain diameter distributions in our samples (Figure 3).

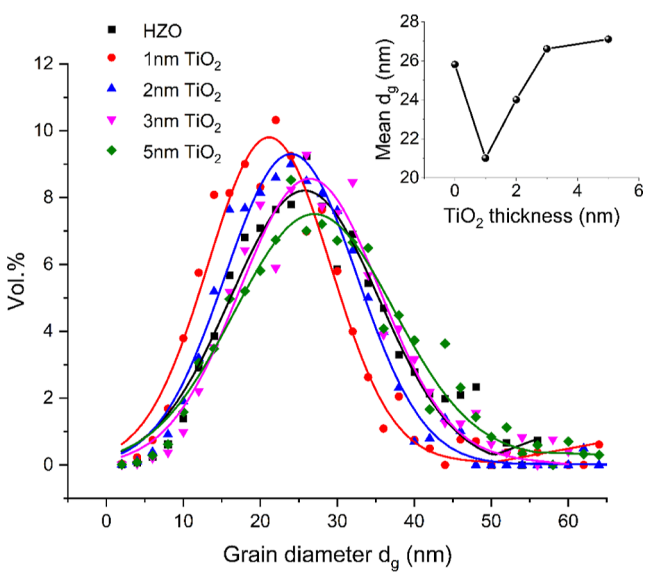

Figure 3. Grain diameters distribution of the HZO grown on the TiN and the TiO_2 (1−5 nm) insets. The grain size was analyzed by applying the watershed method to the contrast-adjusted SEM images (Figure S5 in Supporting Information) for grain segmentation and localization. SEM images were taken from the HZO surfaces after the top TiN removal. The solid lines are the Gaussian fitting curves. The inset shows the mean grain diameter as a function of TiO_2 thickness.

According to the inset in Figure 3, the introduction of the thinnest TiO_2 (1 nm) leads to the decrease of the mean grain diameter of HZO from ∼26 to ∼21 nm, while the mean grain diameter increases again with the rise of TiO_2 thickness, reaching the value ∼26−27 for the thickest TiO_2 (5 nm). Interestingly, the dependence of the mean diameter of the grains on TiO_2 thickness nicely correlates with the trend observed in Figure 1c. Indeed, because the m-phase has a higher surface and lower bulk free energy than o/t-phases, the m-phase is expected to be stable in larger grains, which is observed for the HZO grown directly on TiN and relatively thick TiO_2 (3−5 nm). In contrast, smaller grains of HZO grown on 1−2 nm thick TiO_2 facilitate the o/t-phases formation. Following the interpretation made by Kim et al.[30] and the above-proposed amorphous state of ultrathin TiO_2 (1−2 nm) one can assume that when HZO is grown on the thin amorphous TiO_2 (1−2 nm) it remains amorphous until the subsequent growth of top TiN at 400 °C. In contrast, the anatase TiO_2 (3−5 nm) may facilitate the early nucleation of HZO grains (during HZO growth) due to the crystallographic arguments discussed above, which eventually leads to the growth of larger grains during subsequent growth of the top TiN at 400 °C. The obtained results also make us assume that the TiN surface without an artificially grown TiO_2 inset also can stimulate the earlier nucleation and growth of larger grains as compared to the amorphous ultrathin TiO_2 layers, which underlies the observed higher mean diameter of HZO grains and the higher m-phase content.

One also has to discuss additional effects which can largely influence the crystallization of HZO. Usually, in the process of thermal annealing of HZO films, the TiN electrodes can scavenge O atoms from the HZO layer, generating the V_O in the film.[17] In its turn, it was found that the V_O concentration affects the crystalline structure of the film. The observed tendency is that the increase in the oxygen content in the HZO film leads to stabilization of the m-phase during the annealing process, while the excessive V_O concentration is preferred for the t-phase stabilization. For example, Mittmann et al. showed that the use of the oxide electrodes and the oxygen-rich annealing atmosphere caused the increase in the m-phase content in relation to the o-phase.[40] Another example is the work by Alcala et al., where the increase in the oxygen reactant pulse time also led to the more prominent m-phase stabilization.[41] There is a certain optimum V_O concentration for the maximum o-phase content.[42] In principle, ∼1 nm TiO_2 can weaken oxygen scavenging by the bottom TiN electrode, also contributing to the increase in the o-phase content. Integration of a thicker bottom interfacial layer (3−5 nm) may suppress the scavenging further, contributing to the increase in the m-phase content.

Thus, at this step, the following trends, arising from the cumulative effects of several factors, can be summarized: (1) ultrathin amorphous TiO_2 insets facilitate the decrease of the sizes of HZO grains, resulting in the disappearance of the m-phase and prevent excessive oxygen scavenging, making the o-phase more preferred than t-phase; (2) thicker anatase TiO_2 stimulates o-phase formation because of the local epitaxy but also leads to the growth of larger grains, which cause the adverse increase of m-phase fraction and, probably, hinders the scavenging further, which also may contribute to the higher m-phase fraction. Unfortunately, the experimental confirmation of the evolution of the scavenging is rather challenging because the usually applied X-ray photoelectron spectroscopy is found to be not sensitive to the identification of V_O even in the case without the TiO_2 inset (Figure S6 in Supporting Information) and should be addressed separately in the future.

From a practical point of view, all the changes, induced by TiO_2 bottom insets incorporation in the crystallographic structure of HZO, should strongly affect the ferroelectric

https://doi.org/10.1021/acsomega.2c06237
ACS Omega 2022, 7, 47084−47095

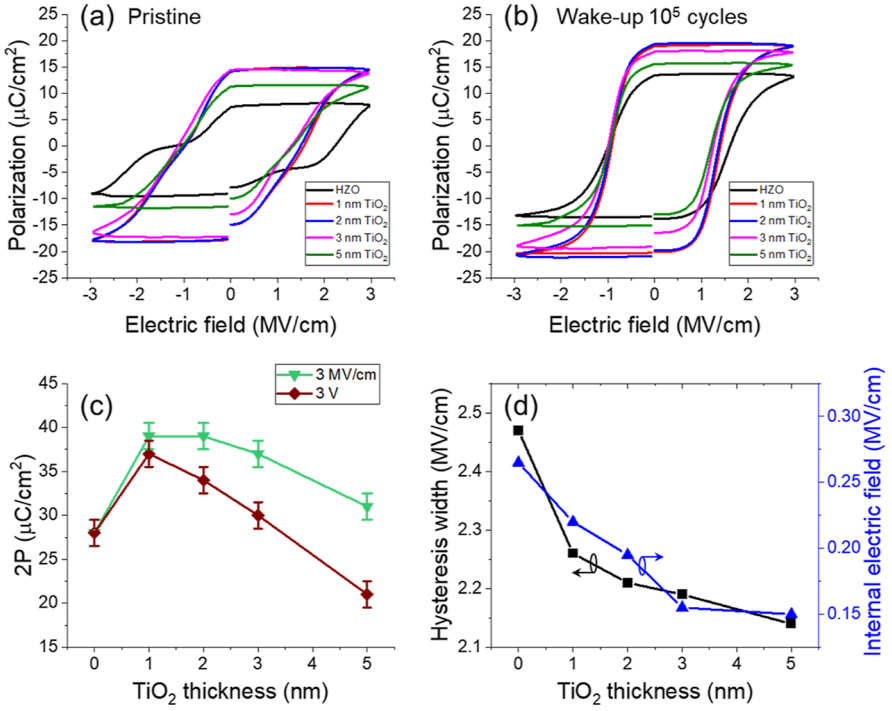

Figure 4. Remanent polarization P_r vs applied electric field curves measured with the E_{HZO} = 3 MV/cm at (a) pristine state and (b) after 10^5 switching cycles. (c) $2P_r$ of woken-up capacitors as a function of the number of TiO_2 ALD cycles measured at conditions of equal E_{HZO} = 3 MV/cm or equal V_{ext} = 3 V. (d) Hysteresis width calculated from the woken-up loops as $|E_c^+| + |E_c^-|$, and the inner field calculated as $(|E_c^+| - |E_c^-|)/2$ as a function of the number of TiO_2 ALD cycles. Lines serve as a guide for the eye.

properties of the devices. It should be noted that because HZO-based capacitors usually demonstrate an increase in the measured $2P_r$ with the rise of the applied electric field,[11,12] it is necessary to compare the $2P_r$ of the different capacitors at the conditions implying the equal electric field for the polarization reversal. Because the total insulator thickness rises with the TiO_2 incorporation and increase of its thickness, the applied external voltage (V_{ext}) required to achieve the equal electric field across the HZO layer (E_{HZO}) should be recalculated as follows

$$V_{ext} = E_{HZO}\frac{\varepsilon_{HZO}d_{TiO_2} + \varepsilon_{TiO_2}d_{HZO}}{\varepsilon_{TiO_2}} \quad (1)$$

where dielectric constants can be evaluated as $\varepsilon_{HZO} \sim 30$ and $\varepsilon_{TiO_2} \sim 42$ for HZO[8] and TiO_2[43] layers, respectively, and the d_{HZO} and d_{TiO_2} are the thicknesses of HZO and TiO_2 layers, respectively. Here, a simple model based on the TiO_2-based and HZO-based capacitors connected in series is applied. According to these calculations, the V_{ext} required to achieve E_{HZO} = 3 MV/cm is equal to 3.2, 3.4, 3.6, and 4 V for the TiN/TiO_2/HZO/TiN capacitors with ∼1, ∼2, ∼3, and ∼5 nm TiO_2, respectively. Thus, the application of such voltages will be implied below when the constant E_{HZO} amplitude of 3 MV/cm will be mentioned. Note that despite the ultrathin TiO_2 interfacial layer exists at the bottom interface of the TiN/HZO/TiN reference structure due to air exposure of the bottom TiN,[25] as shown in Figure S6 in Supporting Information, its thickness after HZO deposition hardly exceeds 0.5 nm, and this layer has not been taken into account in calculations. Therefore, the V_{ext} required to achieve E_{HZO} = 3 MV/cm for the TiN/HZO/TiN reference structure was considered to be 3 V below. In addition, some electrical measurements in this work are also supplemented with the ones performed with constant V_{ext} = 3 V (see Supporting Information).

Figure 4 shows the P_r versus E_{HZO} characteristics at the pristine (Figure 4a) and woken-up (Figure 4b) states for all of the TiN/TiO_2/HZO/TiN structures and TiN/HZO/TiN reference structures, while the E_{HZO} = 3 MV/cm amplitude condition was kept. The "wake-up" procedure involved the application of the 10^5 switching cycles with the pulse duration of t = 3 μs. It can be seen that the pristine hysteresis loop measured from the TiN/HZO/TiN device is pinched, which is attributed to the influence of the t-phase[8] (Figure 4a). Interestingly, in the case of the TiN/TiO_2/HZO/TiN structures, the pinching effect is almost undetectable, which can be linked with the o-phase stabilization evident from the c/a calculations (Figure 1b). After the wake-up, the hysteresis loops are completely depinched due to the transition from the t-phase to the o-phase during field cycling.[44,45]

It can be seen from Figure 4b that the addition of the TiO_2 inset leads to the increase of the $2P_r$ from ∼28 μC/cm² for the TiN/HZO/TiN sample to ∼39 μC/cm² for the woken-up capacitors with ∼1 and ∼2 nm thick TiO_2 bottom insets. However, with the further increase of the TiO_2 layer thickness, the $2P_r$ value decreases. A similar increase in polarization is observed when the measurements are performed at V_{ext} = 3 V (Figure S7 in Supporting Information), though the following decrease is more rapid due to the simultaneous decrease in the effective E_{HZO} related to the rise of the total thickness of the insulating layer discussed above. The observed dependences of the $2P_r$ value on the TiO_2 thickness are summarized in Figure 4c. It is also evident from Figure 4b that the value of the positive coercive field E_c^+ monotonically decreases with the increase of the thickness of the TiO_2 bottom inset, which leads

https://doi.org/10.1021/acsomega.2c06237
ACS Omega 2022, 7, 47084−47095

to the decrease in the total hysteresis width calculated as $|E_c^+| + |E_c^-|$ and in the internal electric field calculated as $(|E_c^+| - |E_c^-|)/2$[46] (Figure 4d).

It can be noticed that the trend in Figure 4c is very similar to the phase change trend observed in Figure 1b,c. Thus, we suppose that, generally, higher $2P_r$ values of the devices with ultrathin TiO_2 are related to the suppression of the m-phase (Figure 1c) and a larger fraction of the o-phase (Figure 1b) in HZO. In turn, a decrease of $2P_r$ with the subsequent increase of TiO_2 film thickness correlates with the increase of the m-phase fraction. A similar trend with the polarization decrease with the increase of inset thickness was also reported for HfO_2[25] and ZrO_2.[26] In addition, this trend was also observed by Kim et al. after the increase in the duration of the ozone treatment of the bottom TiN surface prior to HZO deposition.[32] As was already discussed above, we attribute the m-phase fraction increase to the increase of the mean HZO grain diameter, when it is growing on relatively thick anatase TiO_2 and also to the elimination of the scavenging effect from the bottom TiN. One should note, however, that despite some decrease in $2P_r$ with the increase of TiO_2 thickness, devices with 3−5 nm thick TiO_2 still have higher $2P_r$ than ones without TiO_2 in the constant E_{HZO} conditions. According to the above-mentioned, it is related to the higher o-phase content because of the local epitaxy between the o-phase of HZO and anatase TiO_2.

Next, the retention properties of the TiN/HZO/TiN and TiN/TiO_2/HZO/TiN capacitors were investigated. We used the variation of the procedure by Mueller et al.[4] in which polarization storage is presented by three values: the storage of the same state (SS), the new same state (NSS), and the opposite state (OS). To accelerate the retention loss, the capacitors were baked at T_{bake} = 85 °C for 1, 7, and 50 days between the pulse tests. Figure 5 shows the retention of the SS, NSS, and OS for devices with different thicknesses of the TiO_2 inset (E_{HZO} = 3 MV/cm). It can be seen from Figure 5a,b that the addition of the TiO_2 layer leads to significant improvement in the retention of SS and NSS as compared to the ones of the reference TiN/HZO/TiN structure. In the case of the OS, a monotonic retention improvement can also be observed, especially in the case of OS^- (Figure 5c). It can be noticed that the most noticeable retention improvement is related to the upward polarization (P↑) storage.

Previous studies of the retention in ferroelectric capacitors highlight two main reasons for polarization loss during storage at high temperatures: thermal depolarization and imprint.[47,48] Depolarization fields originated from the nonpolar phases in the bulk of the ferroelectric layer[14] or the screening charges and dead layer at the metal/ferroelectric interface[49] were previously considered as a reason for the retention degradation in HZO- and La/HZO-based structures. Mehmood et al. linked the retention improvement with a reduction of the bulk depolarization fields after the increase of the o-phase fraction.[14] However, in our case, we do not observe a monotonic increase in the o-phase content with the increase of the TiO_2 inset thickness (Figure 1b), and therefore, we cannot tie it with the presented monotonic retention improvement. In turn, Lomenzo et al. demonstrated the increase in the depolarization fields after the integration of the Al_2O_3 dead layer at the TiN/HZO interface.[49] Moreover, the increase in the Al_2O_3 thickness caused a gradual increase in the depolarization fields with the simultaneous retention degradation. According to the "dead layer" model,[50] the depolarization field is inversely

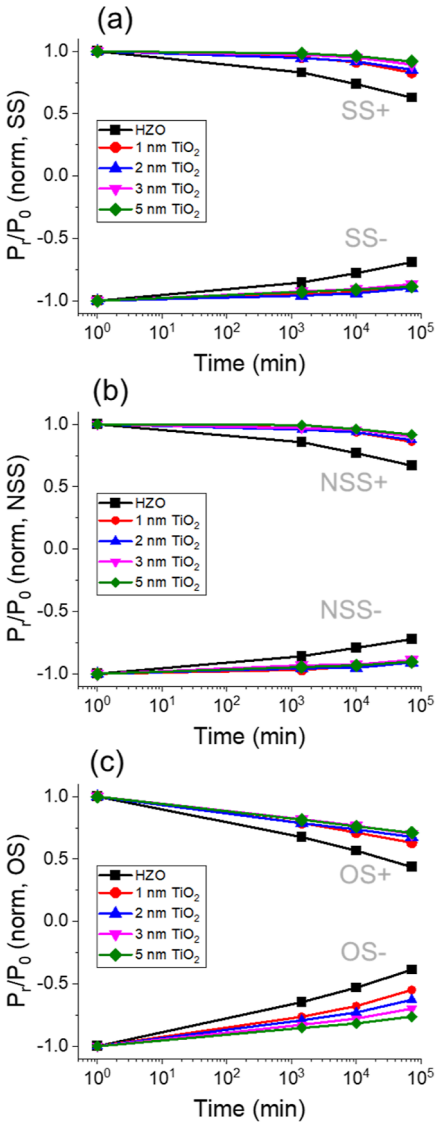

Figure 5. Retention at 85 °C of (a) SS, (b) NSS, and (c) OS states for the upward P↑ (SS^+, NSS^+, and OS^-) and downward P↓ (SS^-, NSS^-, and OS^+) polarization states versus bake time for TiN/HZO/TiN and TiN/TiO_2/HZO/TiN devices. E_{HZO} = 3 MV/cm. Lines serve as a guide for the eye.

proportional to the dielectric permittivity of the interfacial layer

$$E_{dep} = \frac{-P \times d_{int}}{\varepsilon_0(\varepsilon_{FE} d_{int} + \varepsilon_{int} d_{FE})} \quad (2)$$

where P is the measured polarization, ε_{FE} and ε_{int} are dielectric constants of the ferroelectric and interfacial layer, respectively, and the d_{FE} and d_{int} are the thicknesses of the ferroelectric and interfacial layer, respectively. However, from eq 2, because of the difference in the dielectric constant between Al_2O_3 ($\varepsilon \sim 9$)[51] and TiO_2 ($\varepsilon \sim 42$),[43] the magnitude of the depolarization fields should be significantly lower in the case of the TiO_2 inset layer of the same thickness, which can explain the absence of the similar retention degradation in our case.

To confirm this assumption, we carried out measurements that can highlight the depolarization field contribution to the retention loss. For these measurements, the TiN/TiO_2 (5 nm)/HZO/TiN device was chosen for comparison with TiN/

https://doi.org/10.1021/acsomega.2c06237
ACS Omega 2022, 7, 47084−47095

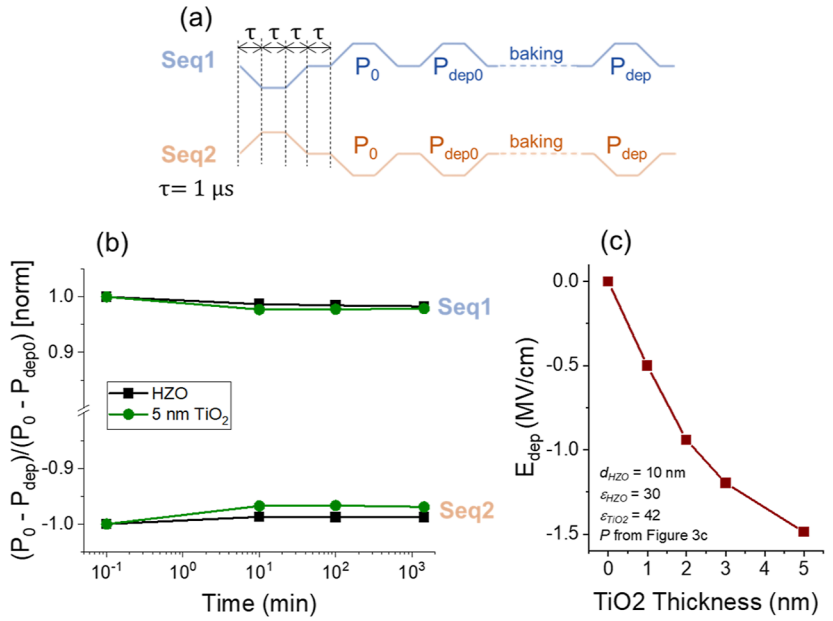

Figure 6. (a) Pulse sequences used for the depolarization contribution analysis. (b) Results of the depolarization-related loss of $2P_r$ measurements performed after different times of storage at 85° from TiN/HZO/TiN and TiN/TiO_2 (5 nm)/HZO/TiN devices. E_{HZO} = 3 MV/cm. Lines serve as a guide for the eye. (c) Depolarization field dependence on the TiO_2 inset thickness calculated from eq 2.

HZO/TiN for maximum clarity since in (2) the depolarization field is directly proportional to the inset layer thickness. The pulse sequences for the measurements are presented in Figure 6a. The first pulse in each of the sequences puts the capacitor in the defined polarization state, upward (P↑) or downward (P↓) for the first (Seq 1) and second sequence (Seq 2), respectively. During the application of the second pulse with the opposite polarity, the $2P_r$ before baking is measured (designated as P_0). During the application of the third pulse with the same polarity, a part of polarization, which could be lost in a short period between the second and third pulse (τ = 1 μs), is measured (designated as P_{dep0}). Finally, the application of the fourth pulse with the same polarity after the different times of baking (10, 100, and 1440 min at 85 °C) allows for measuring the polarization lost because of the depolarization during the baking time (designated as P_{dep}). As a result, the dependency of $(P_0-P_{dep})/(P_0-P_{dep0})$ on the baking time was received, which reflects the part of the polarization which has not been affected by the depolarization effect (Figure 6b). It should be noted that each measured value (P_0, P_{dep0}, and P_{dep}) also contains the contributions from leakages and the difference between the displacement currents at the rise and fall of the related voltage pulses. However, they cancel each other out after mutual subtraction. One also should notice that the differentiation between imprint and depolarization by such an experiment is possible because the state written before the baking becomes even more stable during baking, while the depolarization if it is, affects negatively the stability of the written state.

One can see from Figure 6b that the effect of the depolarization is slightly more pronounced in the case of the TiN/TiO_2 (5 nm)/HZO/TiN device in comparison with the TiN/HZO/TiN device, which is expected according to the theoretical assumptions described above. At the same time, the difference is very insignificant and lies in the area of marginal error. Moreover, the observed depolarization does not change with the baking time at least in the investigated period, which implies the existence of a saturation point similar to one previously reported for PZT.[47] Taking eq 2 into consideration, the effect of the depolarization field on the devices with the thinner TiO_2 inset should be weaker (Figure 6c). In addition, even the strongest depolarization field originating from the 5 nm thick TiO_2 inset does not exceed the coercive field of HZO (~1.5 MV/cm); therefore, it is not sufficient to cause transient polarization loss.[49] This discussion suggests that the observed retention of the TiN/TiO_2/HZO/TiN capacitors should not be significantly affected by the depolarization fields and most likely is determined by the imprint effect.

As was already mentioned, the imprint effect is widely considered to be the main reason for the degradation of the stored polarization in doped HfO_2, especially in the case of OS.[4,5,12,13,52] Therefore, we investigated the evolution of the imprint effect with the increase of the TiO_2 layer thickness. The hysteresis loops measured after baking are shown in Figure S8 in the Supporting Information. Figure 7 shows the imprint shift calculated as E_c^- and E_c^+ shifts from the pristine P_r–E hysteresis. Here, E_{HZO} = 3 MV/cm sweep/pulse

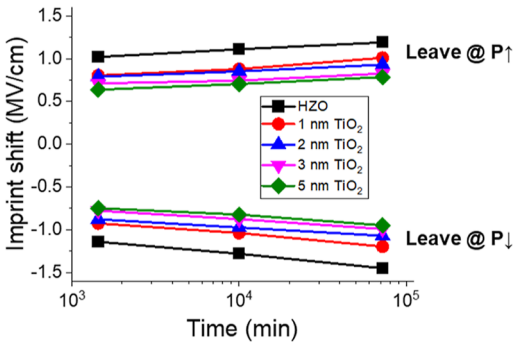

Figure 7. Imprint shift measured from the TiN/HZO/TiN and TiN/TiO_2/HZO/TiN devices at E_{HZO} = 3 MV/cm. Lines serve as a guide for the eye.

https://doi.org/10.1021/acsomega.2c06237
ACS Omega 2022, 7, 47084−47095

amplitude was used for wake-up, poling, and P_r–E measurements. It can be seen that the integration of the TiO_2 layer at the bottom TiN/HZO interface leads to a decrease in the imprint shift. This imprint effect also levels out with the increase of the TiO_2 film thickness in the cases of both P↓ and P↑. Lower imprint can explain the retention improvement observed in Figure 5. The decrease in the hysteresis width observed in Figure 4d also contributes to improved retention, lowering the amount of the domains unavailable for polarization reversal caused by imprint. It is also evident from Figure S8 in the Supporting Information that the effect of back-switching[52] that is observed for the TiN/HZO/TiN capacitors gradually decreases with the increase of the TiO_2 inset thickness. It should also be noted that all capacitors show a smaller imprint shift in the case of P↑ storage, which was previously attributed to the presence of the internal field even prior to sample baking. The decrease in the inner field, evident in Figure 4d, also promotes a slight decrease in the imprint shift asymmetry.

All the aforementioned results imply the large impact of the TiO_2 inset on the retention properties of HZO-based capacitors. As was described in the introduction, the underlying imprint effect is usually assumed to be based on the electrons' injection from the electrode to the V_O in the HZO layer during the polarization storage.[53,54] The shift of the hysteresis loop occurs because of the presence of the electric field across the interfacial layer on the electrode/ferroelectric interface when ferroelectric is poled. We discussed above that incorporation of even the thinnest TiO_2 can hinder the O scavenging from the HZO to TiN, leading to lower V_O content, especially close to the metal/insulator interface. In contrast to the V_O's effect on the crystalline structure, which is characterized by the existence of the optimum V_O content for the o-phase stabilization, the V_O's effect on the retention and imprint should be monotonic. Indeed, we see that even the incorporation of the thinnest TiO_2 improves retention. The increase of the TiO_2 thickness should hinder the scavenging further, which is in accordance with further retention and imprint improvement. It should be noted that the increase of the TiO_2 layer thickness can also suppress the electron injection because of the increase of the barrier width,[12] which leads to a decrease in the electric field across the TiO_2 inset and imprint mitigation.

Finally, it is important to discuss the endurance of TiN/TiO_2/HZO/TiN devices. Figure 8 shows the cycling test results for the TiN/HZO/TiN and TiN/TiO_2 (3 nm)/HZO/TiN structures at the applied electric field amplitude of 3 MV/cm and the pulse duration of 3 μs. Each graph contains five $2P_r$ versus the number of cycles curves to increase the reliability of the endurance claim. The slight decrease in the $2P_r$ value in comparison to the P_r–E_{HZO} curves (Figure 4c) is attributed to the faster measurements. Under these conditions, the TiN/HZO/TiN device endured on average of $\sim 4 \cdot 10^8$ switching cycles before the dielectric breakdown, which is consistent with previous results for the full ALD FE capacitors.[11] One can also observe the wake-up effect up to $\sim 10^5$ cycles, and the fatigue effect lasting from $\sim 10^6$ switching cycles up to the breakdown. On the other hand, the integration of the 3 nm thick TiO_2 inset slightly weakens the endurance, with the average endurance being $\sim 2 \cdot 10^8$ switching cycles. Qualitatively similar to TiN/HZO/TiN, the pronounced wake-up effect takes place up to $\sim 10^6$ cycles; however, no fatigue effect is observed

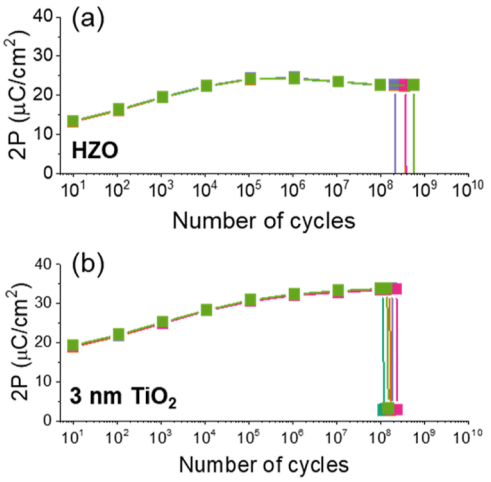

Figure 8. Endurance of TiN/HZO/TiN (a) and TiN/TiO_2 (3 nm)/HZO/TiN (b) capacitors measured by PUND using the applied electric field of 3 MV/cm. The presented graphs contain 5 curves for each device.

afterward. Moreover, the slight gradual increase of remanent polarization continues up until the dielectric breakdown.

Usually, an early breakdown in ferroelectric capacitors is associated with essentially higher leakage current, which is observed at all stages of the device operation.[15] Figure 9a,b shows the leakage current density for the TiN/HZO/TiN and TiN/TiO_2 (3 nm)/HZO/TiN capacitors at the pristine state and after the field cycling. One can see that at the pristine state, the leakages are lower in TiN/TiO_2 (3 nm)/HZO/TiN structures, which is especially prominent at positive voltage polarity, where the current density at V_{read} = 1 V lowers from $\sim 9 \cdot 10^{-7}$ A/cm^2 to $\sim 2 \cdot 10^{-7}$ A/cm^2 with the addition of the TiO_2 inset, that is, by approximately one order of magnitude.

Thus, the origin of the early breakdown of the structures with TiO_2 inset is a more complex phenomenon. To get a deeper insight into this, we analyzed the leakage current after the higher amount of the switching cycles. Figure 9a,b demonstrates also the leakages of the aforementioned structures after 10^5, 10^6, and 10^7 switching cycles. The field cycling was performed at constant E_{HZO} = 3 MV/cm, with the corresponding V_{ext} calculated using eq 1. One can see that leakage current increases with cycling for both structures, which is in principle typical behavior, explained by the generation of additional defects in HZO during cycling.[55] It should be noted that such a generation in the structures with TiO_2 does not contradict the assumption made above, that is, scavenging mitigating, because defect generation can occur at the top interface.[56] However, the more interesting fact is the leakages in the TiN/HZO/TiN structure are rather symmetric with regard to the zero axis at the pristine state and at each stage of cycling, while the ones in TiN/TiO_2 (3 nm)/HZO/TiN transform from the asymmetric to the symmetric ones during the endurance test. We believe that in the second case, the initial asymmetric shape of the curve reflects the influence of TiO_2 on the charge transfer through HZO, and such an influence disappears with cycling. Notably, for the TiN/TiO_2 (3 nm)/HZO/TiN device, the leakage current at the positive polarity after 10^7 switching cycles is ~300 times higher than in the pristine state, while for the TiN/HZO/TiN capacitors, the leakage current increases by 6 times within the same amount of switching cycles. A similar behavior is observed for all the

https://doi.org/10.1021/acsomega.2c06237
ACS Omega 2022, 7, 47084−47095

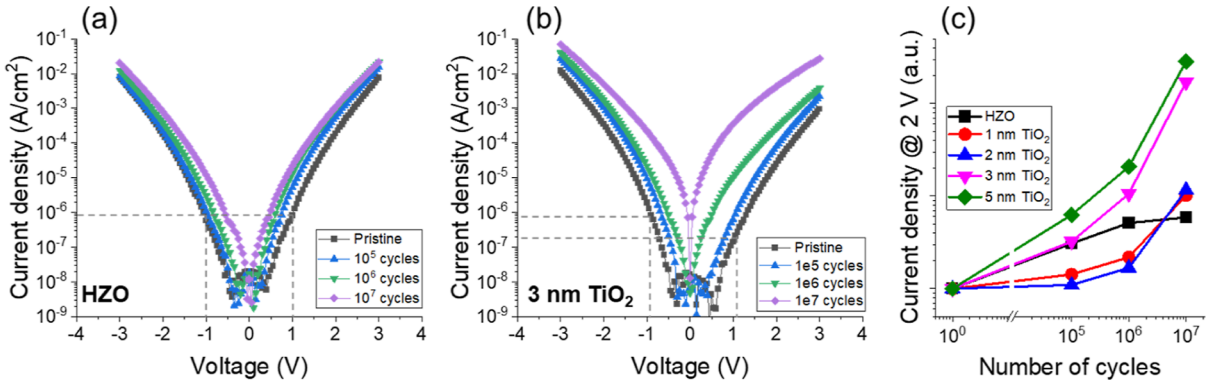

Figure 9. (a) Current density vs voltage curves measured from the TiN/HZO/TiN structure before field cycling (pristine) and after 10^5, 10^6, and 10^7 switching cycles under the applied V_{ext} = 3 V (E_{HZO} = 3 MV/cm). (b) Current density vs voltage curves measured from the TiN/TiO_2 (3 nm)/HZO/TiN structure before field cycling (pristine) and after 10^5, 10^6, and 10^7 switching cycles under the applied V_{ext} = 4 V (E_{HZO} = 3 MV/cm). (c) Normalized leakage current during field cycling for the TiN/HZO/TiN and TiN/TiO_2/HZO/TiN devices measured at the V_{read} = 2 V after 10^5, 10^6, and 10^7 switching cycles under the applied E_{HZO} = 3 MV/cm.

TiN/TiO_2/HZO/TiN devices (Figure S9 in the Supporting Information).

To explain this phenomenon, we propose the following model. As we stated previously, we believe that the integration of the TiO_2 layer mitigates the formation of V_O in the HZO film. However, in this case, the electric field cycling can induce the scavenging of oxygen from the TiO_2 layer by underlying TiN, creating V_O in the TiO_2 inset. According to the previous reports, under external bias, TiO_2 can undergo a reduction reaction and produce the metallically conductive $TiO_{2-n/2}$ phase.[57] This process was also observed by Kwon et al. using HRTEM.[58] We believe that a similar process can occur due to the migration of V_O in TiO_2 under continuous cycling, which can lead to the local transition from stoichiometric TiO_2 to the $TiO_{2-n/2}$ phase.[57,58] In this case, within the frame of the field cycling process, the influence of TiO_2 inset on the current through the HZO is hindered with cycling, so the $I-V$ curve is expected to gradually become more symmetric. At the same time, when the TiO_2 layer becomes more conductive, the electric field across HZO in structures with TiO_2 becomes higher than in TiN/HZO/TiN at the nominally equal E_{HZO} condition described above, because higher voltages are applied to the structures with TiO_2 to achieve the E_{HZO} value of 3 MV/cm. Thus, one can expect more intensive defects generation and more abrupt leakage current rise in the structures with TiO_2 after a certain amount of switching cycles, which is in accordance with Figure 9b.

In addition, since the V_{ext} required to achieve nominally equal E_{HZO} value increases with the increase of TiO_2 thickness, the rate of the leakage current increase should depend on the TiO_2 thickness as well. Figure 9c demonstrates the normalized leakage current through the TiN/HZO/TiN and TiN/TiO_2/HZO/TiN structures measured at the pristine state and after 10^5, 10^6, and 10^7 switching cycles at V_{read} = 2 V. The results observed in this figure also fit the proposed model. Indeed, generally between 10^6 and 10^7 cycles, leakages rise at a much higher rate in the structures with TiO_2 than in the TiN/HZO/TiN, and this effect also becomes more pronounced with the increase of the TiO_2 inset thickness. The different rates of the leakage current increase after 10^5 switching cycles reflect the different conditions of the phase transition and V_O generation in TiO_2 with different thicknesses dependent on the V_{ext} value.

The proposed model can also explain the absence of the fatigue effect after TiO_2 integration. Generally, the decrease in remanent polarization after a certain amount of switching cycles is attributed to the charge trapping at the defect sites, which can be located mostly at the domains' walls or interfaces, leading to the domains' walls pinning or seeds' inhibition and consequently suppressing of the switchable polarization.[59] However, in the case of the TiO_2/HZO bilayer, the fatigue-related decrease in the electric field is compensated by the increase in the E_{HZO} after the TiO_2 phase transition and the related involvement of the additional, harder domains in the polarization reversal. In other words, the wake-up effect[15] is believed to continue and overlap with the potential fatigue effect. Hence, we can see even a slight increase in the $2P_r$ value up until the breakdown of the HZO layer, especially in the case of the thickest TiO_2 inset.

4. CONCLUSIONS

In this article, the influence of the TiO_2 inset on the ferroelectric properties of HZO-based capacitors was investigated. We showed that the presence of the TiO_2 seed layer at the bottom TiN/HZO interface significantly affects the crystalline structure of the HZO film. These changes, in turn, influenced the ferroelectricity in TiN/TiO_2/HZO/TiN structures, inducing the notable polarization increase. We also carefully investigated the retention properties of TiN/TiO_2/HZO/TiN structures and found out that the integration of the TiO_2 layers greatly improved the polarization storage ability. Analyzing the depolarization contribution to the retention loss, we concluded that the retention in TiN/TiO_2/HZO/TiN structures is determined by the imprint effect. We believe that the decrease in the oxygen vacancy concentration plays a key role in retention improvement and imprint mitigation. On the other hand, we observed that the endurance of the TiN/TiO_2/HZO/TiN structures measured with an equal applied electric field is only slightly weakened as compared with the TiN/HZO/TiN ones. The reason for the weakness is a more rapid leakage current increase during the field cycling process. This behavior is attributed to the increase in the effective electric field in the HZO layer due to the local transition from stoichiometric TiO_2 to the $TiO_{2-n/2}$ phase. However, the endurance of TiN/TiO_2/HZO/TiN structures is still comparable with that of the TiN/HZO/TiN devices, which, along with the significant retention improvement, makes the insertion of the TiO_2 interfacial layer at the bottom interface

https://doi.org/10.1021/acsomega.2c06237
ACS Omega 2022, 7, 47084−47095

very promising for possible technological integration, allowing one to achieve high retention without much deterioration in endurance.

■ ASSOCIATED CONTENT

Supporting Information

The Supporting Information is available free of charge at https://pubs.acs.org/doi/10.1021/acsomega.2c06237.

Pulse scheme for the retention measurements; TEM measurements of the structures with ultrathin TiO_2 films; SEM measurements for grain size evaluation; XPS investigations; electrical measurements at V_{ext} = 3 V; imprint hysteresis loop measurements; and leakage current measurements for all TiO_2 thicknesses (PDF)

■ AUTHOR INFORMATION

Corresponding Author

Andrey M. Markeev − *Moscow Institute of Physics and Technology, Moscow Region 141700, Russia;* orcid.org/0000-0001-6777-5706; Email: markeev.am@mipt.ru

Authors

Aleksandra A. Koroleva − *Moscow Institute of Physics and Technology, Moscow Region 141700, Russia*

Anna G. Chernikova − *Moscow Institute of Physics and Technology, Moscow Region 141700, Russia;* orcid.org/0000-0002-9783-6159

Sergei S. Zarubin − *Moscow Institute of Physics and Technology, Moscow Region 141700, Russia*

Evgeny Korostylev − *Moscow Institute of Physics and Technology, Moscow Region 141700, Russia*

Roman R. Khakimov − *Moscow Institute of Physics and Technology, Moscow Region 141700, Russia*

Maksim Yu. Zhuk − *Moscow Institute of Physics and Technology, Moscow Region 141700, Russia*

Complete contact information is available at: https://pubs.acs.org/10.1021/acsomega.2c06237

Notes

The authors declare no competing financial interest.

■ ACKNOWLEDGMENTS

XRD, TEM, and SEM measurements, depolarization, and imprint effect investigations were supported by the Russian Science Foundation (Project. No 18-19-00527). Ferroelectric response, endurance, and retention property investigations were supported by the Foundation for Advanced Research (Project "Magnit"). The authors also acknowledge the MIPT Shared Facilities Center supported by the Ministry of Education and Science of the Russian Federation for access to the equipment.

■ REFERENCES

(1) Böscke, T. S.; Müller, J.; Bräuhaus, D.; Schröder, U.; Böttger, U. Ferroelectricity in Hafnium Oxide Thin Films. *Appl. Phys. Lett.* **2011**, *99*, 102903.

(2) Chernikova, A.; Kozodaev, M.; Markeev, A.; Negrov, D.; Spiridonov, M.; Zarubin, S.; Bak, O.; Buragohain, P.; Lu, H.; Suvorova, E.; Gruverman, A.; Zenkevich, A. Ultrathin Hf0.5Zr0.5O2 Ferroelectric Films on Si. *ACS Appl. Mater. Interfaces* **2016**, *8*, 7232−7237.

(3) Kim, S. J.; Mohan, J.; Summerfelt, S. R.; Kim, J. Ferroelectric Hf0.5Zr0.5O2 Thin Films: A Review of Recent Advances. *JOM* **2019**, *71*, 246−255.

(4) Mueller, S.; Muller, J.; Schroeder, U.; Mikolajick, T. Reliability Characteristics of Ferroelectric Si:HfO2 Thin Films for Memory Applications. *IEEE Trans. Device Mater. Reliab.* **2013**, *13*, 93−97.

(5) Florent, K.; Lavizzari, S.; Di Piazza, L.; Popovici, M.; Duan, J.; Groeseneken, G.; Van Houdt, J. Reliability Study of Ferroelectric Al:HfO2 Thin Films for DRAM and NAND Applications. *IEEE Trans. Electron Devices* **2017**, *64*, 4091−4098.

(6) Kozodaev, M. G.; Chernikova, A. G.; Korostylev, E. V.; Park, M. H.; Schroeder, U.; Hwang, C. S.; Markeev, A. M. Ferroelectric Properties of Lightly Doped La:HfO2 Thin Films Grown by Plasma-Assisted Atomic Layer Deposition. *Appl. Phys. Lett.* **2017**, *111*, 132903.

(7) Shimizu, T.; Katayama, K.; Kiguchi, T.; Akama, A.; Konno, T. J.; Sakata, O.; Funakubo, H. The Demonstration of Significant Ferroelectricity in Epitaxial Y-Doped HfO2 Film. *Sci. Rep.* **2016**, *6*, 1−8.

(8) Müller, J.; Böscke, T. S.; Schröder, U.; Mueller, S.; Bräuhaus, D.; Böttger, U.; Frey, L.; Mikolajick, T. Ferroelectricity in Simple Binary ZrO2 and HfO2. *Nano Lett.* **2012**, *12*, 4318−4323.

(9) Kozodaev, M. G.; Lebedinskii, Y. Y.; Chernikova, A. G.; Polyakov, S. N.; Markeev, A. M. Low Temperature Plasma-Enhanced ALD TiN Ultrathin Films for Hf0.5Zr0.5O2 -Based Ferroelectric MIM Structures. *Phys. Status Solidi* **2017**, *214*, 1700056.

(10) Zarubin, S.; Suvorova, E.; Spiridonov, M.; Negrov, D.; Chernikova, A.; Markeev, A.; Zenkevich, A. Fully ALD-Grown TiN/Hf0.5Zr0.5O2/TiN Stacks: Ferroelectric and Structural Properties. *Appl. Phys. Lett.* **2016**, *109*, 192903.

(11) Kozodaev, M. G.; Chernikova, A. G.; Korostylev, E. V.; Park, M. H.; Khakimov, R. R.; Hwang, C. S.; Markeev, A. M. Mitigating Wakeup Effect and Improving Endurance of Ferroelectric HfO2 -ZrO2 Thin Films by Careful La-Doping. *J. Appl. Phys.* **2019**, *125*, 034101.

(12) Khakimov, R. R.; Chernikova, A. G.; Lebedinskii, Y.; Koroleva, A. A.; Markeev, A. M. Influence of the Annealing Temperature and Applied Electric Field on the Reliability of TiN/Hf0.5Zr0.5O2/TiN Capacitors. *ACS Appl. Electron. Mater.* **2021**, *3*, 4317−4327.

(13) Chouprik, A.; Kondratyuk, E.; Mikheev, V.; Matveyev, Y.; Spiridonov, M.; Chernikova, A.; Kozodaev, M. G.; Markeev, A. M.; Zenkevich, A.; Negrov, D. Origin of the Retention Loss in Ferroelectric Hf0.5Zr0.5O2-Based Memory Devices. *Acta Mater.* **2021**, *204*, 116515.

(14) Mehmood, F.; Hoffmann, M.; Lomenzo, P. D.; Richter, C.; Materano, M.; Mikolajick, T.; Schroeder, U. Bulk Depolarization Fields as a Major Contributor to the Ferroelectric Reliability Performance in Lanthanum Doped Hf0.5Zr0.5O2 Capacitors. *Adv. Mater. Interfaces* **2019**, *6*, 1901180.

(15) Pešić, M.; Fengler, F. P. G.; Larcher, L.; Padovani, A.; Schenk, T.; Grimley, E. D.; Sang, X.; LeBeau, J. M.; Slesazeck, S.; Schroeder, U.; Mikolajick, T. Physical Mechanisms behind the Field-Cycling Behavior of HfO2 -Based Ferroelectric Capacitors. *Adv. Funct. Mater.* **2016**, *26*, 4601−4612.

(16) Fengler, F. P. G.; Hoffmann, M.; Slesazeck, S.; Mikolajick, T.; Schroeder, U. On the Relationship between Field Cycling and Imprint in Ferroelectric Hf0.5Zr0.5O2. *J. Appl. Phys.* **2018**, *123*, 204101.

(17) Hamouda, W.; Pancotti, A.; Lubin, C.; Tortech, L.; Richter, C.; Mikolajick, T.; Schroeder, U.; Barrett, N. Physical Chemistry of the TiN/Hf0.5Zr0.5O2 Interface. *J. Appl. Phys.* **2020**, *127*, 064105.

(18) Tagantsev, A. K.; Gerra, G. Interface-Induced Phenomena in Polarization Response of Ferroelectric Thin Films. *J. Appl. Phys.* **2006**, *100*, 051607.

(19) He, G.; Chen, X.; Sun, Z. Interface Engineering and Chemistry of Hf-Based High-k Dielectrics on III−V Substrates. *Surf. Sci. Rep.* **2013**, *68*, 68−107.

(20) Gao, J.; He, G.; Xiao, D.; Jin, P.; Jiang, S.; Li, W.; Liang, S.; Zhu, L. Passivation of Ge Surface Treated with Trimethylaluminum

and Investigation of Electrical Properties of HfTiO/Ge Gate Stacks. *J. Mater. Sci. Technol.* **2017**, *33*, 901−906.
(21) Zhang, J. W.; He, G.; Zhou, L.; Chen, H. S.; Chen, X. S.; Chen, X. F.; Deng, B.; Lv, J. G.; Sun, Z. Q. Microstructure Optimization and Optical and Interfacial Properties Modulation of Sputtering-Derived HfO2 Thin Films by TiO2 Incorporation. *J. Alloys Compd.* **2014**, *611*, 253−259.
(22) He, G.; Gao, J.; Chen, H.; Cui, J.; Sun, Z.; Chen, X. Modulating the Interface Quality and Electrical Properties of HfTiO/InGaAs Gate Stack by Atomic-Layer-Deposition-Derived Al2O3 Passivation Layer. *ACS Appl. Mater. Interfaces* **2014**, *6*, 22013−22025.
(23) Onaya, T.; Nabatame, T.; Sawamoto, N.; Ohi, A.; Ikeda, N.; Nagata, T.; Ogura, A. Improvement in Ferroelectricity of HfxZr1-xO2 Thin Films Using Top- and Bottom-ZrO2 Nucleation Layers. *APL Mater.* **2019**, *7*, 061107.
(24) Gaddam, V.; Das, D.; Jung, T.; Jeon, S. Ferroelectricity Enhancement in Hf0.5Zr0.5O2 Based Tri-Layer Capacitors at Low-Temperature (350 °C) Annealing Process. *IEEE Electron Device Lett.* **2021**, *42*, 812−815.
(25) Gaddam, V.; Das, D.; Jeon, S. Insertion of HfO2 Seed/Dielectric Layer to the Ferroelectric HZO Films for Heightened Remanent Polarization in MFM Capacitors. *IEEE Trans. Electron Devices* **2020**, *67*, 745−750.
(26) Onaya, T.; Nabatame, T.; Sawamoto, N.; Ohi, A.; Ikeda, N.; Chikyow, T.; Ogura, A. Improvement in Ferroelectricity of HfxZr1−xO2 Thin Films Using ZrO2 Seed Layer. *Appl. Phys. Express* **2017**, *10*, 081501.
(27) Lee, S. J.; Kim, M. J.; Lee, T. Y.; Lee, T. I.; Bong, J. H.; Shin, S. W.; Kim, S. H.; Hwang, W. S.; Cho, B. J. Effect of ZrO2 Interfacial Layer on Forming Ferroelectric HfxZryOz on Si Substrate. *AIP Adv.* **2019**, *9*, 125020.
(28) Liu, B.; Cao, Y.; Zhang, W.; Li, Y. Excellent Ferroelectric Hf0.5Zr0.5O2 thin Films with Ultra-Thin Al2O3 serving as Capping Layer. *Appl. Phys. Lett.* **2021**, *119*, 172902.
(29) Lee, J.; Song, M. S.; Jang, W. S.; Byun, J.; Lee, H.; Park, M. H.; Lee, J.; Kim, Y. M.; Chae, S. C.; Choi, T. Modulating the Ferroelectricity of Hafnium Zirconium Oxide Ultrathin Films via Interface Engineering to Control the Oxygen Vacancy Distribution. *Adv. Mater. Interfaces* **2022**, *9*, 2101647.
(30) Kim, B. Y.; Park, H. W.; Hyun, S. D.; Lee, Y. B.; Lee, S. H.; Oh, M.; Ryoo, S. K.; Lee, I. S.; Byun, S.; Shim, D.; Cho, D.; Park, M. H.; Hwang, C. S. Enhanced Ferroelectric Properties in Hf0.5Zr0.5O2 Films Using a HfO0.61N0.72 Interfacial Layer. *Adv. Electron. Mater.* **2022**, *8*, 2100042.
(31) Kim, B. Y.; Kim, S. H.; Park, H. W.; Lee, Y. B.; Lee, S. H.; Oh, M.; Ryoo, S. K.; Lee, I. S.; Byun, S.; Shim, D.; Park, M. H.; Hwang, C. S. Improved Ferroelectricity in Hf0.5Zr0.5O2 by Inserting an Upper HfOxNy Interfacial Layer. *Appl. Phys. Lett.* **2021**, *119*, 122902.
(32) Kim, H.; Dae, K. S.; Oh, Y.; Lee, S.; Lee, Y.; Ahn, S.; Jang, J. H.; Ahn, J. A Simple Strategy to Realize Super Stable Ferroelectric Capacitor via Interface Engineering. *Adv. Mater. Interfaces* **2022**, *9*, 2102528.
(33) Qi, Y.; Xu, X.; Krylov, I.; Eizenberg, M. Ferroelectricity of As-Deposited HZO Fabricated by Plasma-Enhanced Atomic Layer Deposition at 300 °C by Inserting TiO2 interlayers. *Appl. Phys. Lett.* **2021**, *118*, 032906.
(34) Gaddam, V.; Das, D.; Jung, T.; Jeon, S. Ferroelectricity Enhancement in Hf0.5Zr0.5O2 Based Tri-Layer Capacitors at Low-Temperature (350 °C) Annealing Process. *IEEE Electron Device Lett.* **2021**, *42*, 812−815.
(35) Stadelmann, P. A. EMS—a software package for electron diffraction analysis and HREM image simulation in materials science. *Ultramicroscopy* **1987**, *21*, 131−145.
(36) Hyuk Park, M.; Joon Kim, H.; Jin Kim, Y.; Lee, W.; Moon, T.; Seong Hwang, C. Evolution of Phases and Ferroelectric Properties of Thin Hf0.5Zr0.5O2 Films According to the Thickness and Annealing Temperature. *Appl. Phys. Lett.* **2013**, *102*, 242905.
(37) Park, M. H.; Lee, Y. H.; Kim, H. J.; Kim, Y. J.; Moon, T.; Kim, K. D.; Hyun, S. D.; Mikolajick, T.; Schroeder, U.; Hwang, C. S. Understanding the Formation of the Metastable Ferroelectric Phase in Hafnia−Zirconia Solid Solution Thin Films. *Nanoscale* **2018**, *10*, 716−725.
(38) Niemelä, J. P.; Marin, G.; Karppinen, M. Titanium Dioxide Thin Films by Atomic Layer Deposition: A Review. *Semicond. Sci. Technol.* **2017**, *32*, 093005.
(39) Szilágyi, I. M.; Santala, E.; Heikkilä, M.; Pore, V.; Kemell, M.; Nikitin, T.; Teucher, G.; Firkala, T.; Khriachtchev, L.; Räsänen, M.; Ritala, M.; Leskelä, M. Photocatalytic Properties of WO3/TiO2 Core/Shell Nanofibers Prepared by Electrospinning and Atomic Layer Deposition. *Chem. Vap. Depos.* **2013**, *19*, 149−155.
(40) Mittmann, T.; Szyjka, T.; Alex, H.; Istrate, M. C.; Lomenzo, P. D.; Baumgarten, L.; Müller, M.; Jones, J. L.; Pintilie, L.; Mikolajick, T.; Schroeder, U. Impact of Iridium Oxide Electrodes on the Ferroelectric Phase of Thin Hf0.5Zr0.5O2 Films. *Phys. Status Solidi Rapid Res. Lett.* **2021**, *15*, 2100012.
(41) Alcala, R.; Richter, C.; Materano, M.; Lomenzo, P. D.; Zhou, C.; Jones, J. L.; Mikolajick, T.; Schroeder, U. Influence of Oxygen Source on the Ferroelectric Properties of ALD Grown Hf1-xZrxO2 Films. *J. Phys. D Appl. Phys.* **2021**, *54*, 035102.
(42) Materano, M.; Lomenzo, P. D.; Kersch, A.; Park, M. H.; Mikolajick, T.; Schroeder, U. Interplay between Oxygen Defects and Dopants: Effect on Structure and Performance of HfO2 -Based Ferroelectrics. *Inorg. Chem. Front.* **2021**, *8*, 2650−2672.
(43) Choi, G.-J.; Kim, S. K.; Lee, S. Y.; Park, W. Y.; Seo, M.; Choi, B. J.; Hwang, C. S. Atomic Layer Deposition of TiO2 Films on Ru Buffered TiN Electrode for Capacitor Applications. *J. Electrochem. Soc.* **2009**, *156*, G71.
(44) Schenk, T.; Schroeder, U.; Pešić, M.; Popovici, M.; Pershin, Y. V.; Mikolajick, T. Electric Field Cycling Behavior of Ferroelectric Hafnium Oxide. *ACS Appl. Mater. Interfaces* **2014**, *6*, 19744−19751.
(45) Grimley, E. D.; Schenk, T.; Sang, X.; Pešić, M.; Schroeder, U.; Mikolajick, T.; LeBeau, J. M. Structural Changes Underlying Field-Cycling Phenomena in Ferroelectric HfO2 Thin Films. *Adv. Electron. Mater.* **2016**, *2*, 1600173.
(46) Kim, B. Y.; Kim, B. S.; Hyun, S. D.; Kim, H. H.; Lee, Y. B.; Park, H. W.; Park, M. H.; Hwang, C. S. Study of Ferroelectric Characteristics of Hf0.5Zr0.5O2 Thin Films Grown on Sputtered or Atomic-Layer-Deposited TiN Bottom Electrodes. *Appl. Phys. Lett.* **2020**, *117*, 022902.
(47) Rodriguez, J. A.; Remack, K.; Boku, K.; Udayakumar, K. R.; Aggarwal, S.; Summerfelt, S. R.; Celii, F. G.; Martin, S.; Hall, L.; Taylor, K.; Moise, T.; McAdams, H.; McPherson, J.; Bailey, R.; Fox, G.; Depner, M. Reliability Properties of Low-Voltage Ferroelectric Capacitors and Memory Arrays. *IEEE Trans. Device Mater. Reliab.* **2004**, *4*, 436−449.
(48) Rodriguez, J.; Remack, K.; Gertas, J.; Wang, L.; Zhou, C.; Boku, K.; Rodriguez-Latorre, J.; Udayakumar, K. R.; Summerfelt, S.; Moise, T.; Kim, D.; Groat, J.; Eliason, J.; Depner, M.; Chu, F.Reliability of Ferroelectric Random Access Memory Embedded within 130nm CMOS. *IEEE International Reliability Physics Symposium*; IEEE, 2010; pp 750−758.
(49) Lomenzo, P. D.; Slesazeck, S.; Hoffmann, M.; Mikolajick, T.; Schroeder, U.; Max, B.; Mikolajick, T.Ferroelectric Hf1-x ZrxO2 Memories: Device Reliability and Depolarization Fields. *2019 19th Non-Volatile Memory Technology Symposium (NVMTS)*; IEEE, 2019; pp 1−8.
(50) Lomenzo, P. D.; Richter, C.; Mikolajick, T.; Schroeder, U. Depolarization as Driving Force in Antiferroelectric Hafnia and Ferroelectric Wake-Up. *ACS Appl. Electron. Mater.* **2020**, *2*, 1583−1595.
(51) Acharya, J.; Wilt, J.; Liu, B.; Wu, J. Probing the Dielectric Properties of Ultrathin Al/Al2O3/Al Trilayers Fabricated Using in Situ Sputtering and Atomic Layer Deposition. *ACS Appl. Mater. Interfaces* **2018**, *10*, 3112−3120.
(52) Chernikova, A. G.; Markeev, A. M. Dynamic Imprint Recovery as an Origin of the Pulse Width Dependence of Retention in Hf0.5Zr0.5O2 -Based Capacitors. *Appl. Phys. Lett.* **2021**, *119*, 032904.

https://doi.org/10.1021/acsomega.2c06237
ACS Omega 2022, 7, 47084−47095

(53) Fengler, F. P. G.; Pešić, M.; Starschich, S.; Schneller, T.; Künneth, C.; Böttger, U.; Mulaosmanovic, H.; Schenk, T.; Park, M. H.; Nigon, R.; Muralt, P.; Mikolajick, T.; Schroeder, U. Domain Pinning: Comparison of Hafnia and PZT Based Ferroelectrics. *Adv. Electron. Mater.* **2017**, *3*, 1600505.
(54) Higashi, Y.; Florent, K.; Subirats, A.; Kaczer, B.; Di Piazza, L.; Clima, S.; Ronchi, N.; McMitchell, S. R. C.; Banerjee, K.; Celano, U.; Suzuki, M.; Linten, D.; Van Houdt, J.New Insights into the Imprint Effect in FE-HfO2 and Its Recovery. *IEEE International Reliability Physics Symposium (IRPS)*; IEEE, 2019, 2019-March; pp 1−7.
(55) Pesic, M.; Fengler, F. P. G.; Slesazeck, S.; Schroeder, U.; Mikolajick, T.; Larcher, L.; Padovani, A.Root Cause of Degradation in Novel HfO2-Based Ferroelectric Memories. *2016 IEEE International Reliability Physics Symposium (IRPS)*; IEEE, 2016; Vol. *2016*-Septe, p MY-3-1-MY-3-5.
(56) Hamouda, W.; Mehmood, F.; Mikolajick, T.; Schroeder, U.; Mentes, T. O.; Locatelli, A.; Barrett, N. Oxygen Vacancy Concentration as a Function of Cycling and Polarization State in TiN/Hf0.5Zr0.5O2/TiN Ferroelectric Capacitors Studied by x-Ray Photoemission Electron Microscopy. *Appl. Phys. Lett.* **2022**, *120*, 202902.
(57) Waser, R.; Aono, M.Nanoionics-Based Resistive Switching Memories. In *Nanoscience and Technology*; Co-Published with Macmillan Publishers Ltd: U.K., 2009; pp 158−165.
(58) Kwon, D.-H.; Kim, K. M.; Jang, J. H.; Jeon, J. M.; Lee, M. H.; Kim, G. H.; Li, X.-S.; Park, G.-S.; Lee, B.; Han, S.; Kim, M.; Hwang, C. S. Atomic Structure of Conducting Nanofilaments in TiO2 Resistive Switching Memory. *Nat. Nanotechnol.* **2010**, *5*, 148−153.
(59) Colla, E. L.; Taylor, D. V.; Tagantsev, A. K.; Setter, N. Discrimination between Bulk and Interface Scenarios for the Suppression of the Switchable Polarization (Fatigue) in Pb(Zr,Ti)O3 Thin Films Capacitors with Pt Electrodes. *Appl. Phys. Lett.* **1998**, *72*, 2478−2480.

https://doi.org/10.1021/acsomega.2c06237
ACS Omega 2022, 7, 47084−47095